buildings

Article

Static and Dynamic Response Analysis of Flexible Photovoltaic Mounts

Yibing Lou, Jian Zhang * and Yuxin Pan

School of Shipbuilding and Ocean Engineering, Jiangsu University of Science and Technology, Zhenjiang 212100, China; 13270323596@163.com (Y.L.); pyx18360735895@163.com (Y.P.)
* Correspondence: justzj@just.edu.cn

Abstract: Traditional rigid photovoltaic (PV) support structures exhibit several limitations during operational deployment. Therefore, flexible PV mounting systems have been developed. These flexible PV supports, characterized by their heightened sensitivity to wind loading, necessitate a thorough analysis of their static and dynamic responses. This study involves the development of a MATLAB code to simulate the fluctuating wind load time series and the subsequent structural modeling in SAP2000 to evaluate the safety performance of flexible PV supports under extreme wind conditions. The research explores the critical wind speeds relative to varying spans and prestress levels within the system. Modal analysis reveals that the flexible PV support structures do not experience resonant frequencies that could amplify oscillations. The analysis also provides insights into the mode shapes of these structures. An analysis of the wind-induced vibration responses of the flexible PV support structures was conducted. The results indicated that the mid-span displacements and the axial forces in the wind-resistant cables are greater under wind-pressure conditions compared to wind-suction conditions. Conversely, for mid-span accelerations, the wind-suction conditions resulted in higher values than the wind-pressure conditions. Furthermore, the wind-induced vibration coefficients were computed, with findings suggesting a recommended coefficient range of 1.5 to 2.52. To mitigate wind-induced vibrations, structural reinforcement strategies were assessed. The results indicate that the introduction of support beams at the mid-span is the most effective measure to attenuate wind-induced vibrational responses. Conversely, increasing the diameter of the tensioned cables exhibited a negligible effect in reducing these responses. On the other hand, implementing stabilizing cables at the mid-span demonstrated a substantial reduction in wind-induced vibrational responses under suction wind-load conditions.

Keywords: flexible photovoltaic mounts; wind-vibration response; static response; fluctuating wind; wind-vibration coefficient

check for updates

Citation: Lou, Y.; Zhang, J.; Pan, Y. Static and Dynamic Response Analysis of Flexible Photovoltaic Mounts. *Buildings* **2024**, *14*, 2037. https://doi.org/10.3390/buildings14072037

Academic Editor: Humberto Varum

Received: 11 June 2024
Revised: 26 June 2024
Accepted: 29 June 2024
Published: 4 July 2024

1. Introduction

Since the 18th National Congress of the Communist Party of China, China has entered a new phase of development, and the energy sector has likewise reached a critical period of transformation [1]. Renewable energy, particularly solar PV power, is increasingly becoming a key focus in the global energy structure transition. China boasts exceptionally favorable conditions for PV power generation [2,3], with more than 66% of its regions receiving over 200 h of sunlight annually [4]. The traditional rigid PV support systems face several issues and limitations, such as the requirement for large land areas, which constrain their deployment and development, especially in eastern regions [5]. In response to these challenges, flexible PV support systems have rapidly developed. Compared to conventional rigid PV supports, flexible PV supports offer advantages such as flexibility, adaptability, shorter construction periods, lower costs, and higher land utilization rates [6].

Previous research has primarily focused on simulating wind loads on PV panels, with numerous numerical simulations conducted by researchers [7–12]. Additionally, various scholars have examined rooftop PV structures, exploring the effects of the tilt angle, array spacing, building type, and parapet on the wind action on rooftop PV arrays [13–16].

Fluctuating wind is caused by the irregularity of the wind, with its intensity randomly varying over time. There are many methods to simulate wind load time series, such as the linear filter method [17,18], harmonic superposition method [19,20], inverse Fourier transform method [21], wavelet analysis method [22,23], and artificial neural network method [24,25]. Among these methods, the autoregressive (AR) model is widely used in stochastic vibration and time series analysis due to its high computational efficiency and simplicity. The AR model generates a random process for wind speed by constructing one or more autoregressive terms to describe the relationship between the current wind speed value and its historical values. When simulating the fluctuating wind speed time series for flexible PV supports, the AR model's characteristics can be used to generate time series data that match the actual wind speed characteristics, providing a basis for wind load analysis of the structure.

Flexible PV supports are highly sensitive to fluctuating wind, and thus numerous scholars have studied the wind-induced response of flexible PV supports. Guo Tao [26] and others, in conjunction with actual engineering projects, discovered that the maximum amplitude of the wind-induced response of PV arrays was approximately 8.0 cm. Cai Yuan [27] and colleagues researched the wind resistance design methods for flexible PV support structures, deriving a formula to estimate the standard deviation of the wind-induced dynamic response by using the standard deviation of the quasi-static response of the structure, and validated the accuracy of this formula. Xie Dan [28], Wang Zeguo [29], and their respective teams used finite element software to study the natural vibration characteristics and wind-induced response of single-layer cable-supported flexible PV support structures. They found that the structure is prone to vertical vibration and torsional deformation, and that fluctuating wind vibration has little effect on structural deflection under transverse wind loads. Xu [30] and others conducted a series of wind tunnel tests on flexible PV supports and found that the torsional vibration of flexible PV supports is significant, with PV modules being most at risk when the wind direction angle is 180°. Xu [31] and his team further conducted wind tunnel tests using aeroelastic and rigid models, showing that the vertical vibration of flexible cable-supported PV systems increases significantly with the tilt angle, and that the gust load coefficient of PV panels with a tilt angle of 10° ranges between 1.2 and 2.5. Liu [32] and colleagues investigated the wind-induced response and critical wind speed of a 33-m span flexible PV support structure through wind tunnel tests based on elastic models, finding that 180° and 0° are the most unfavorable wind directions, with a critical wind speed of approximately 18.5 m/s, and examined the effectiveness of three measures to mitigate wind-induced vibrations. Li [33] and his team studied the instability mechanisms and failure criteria of large-span flexible PV supports, concluding that triangular and cross diagonal braces fail at critical wind speeds of 51 m/s and 46 m/s, respectively.

2. Materials and Methods

2.1. Flexible PV Mounting Structure Geometric Model

The constructed flexible PV support model consists of six spans, each with a span of 2 m. The spans are connected by struts, with the support cables having a height of 4.75 m, directly supporting the PV panels. The wind-resistant cables are 4 m high and are connected to the lower ends of the struts. The end support beams are 4 m high, with tie rods connected to the end support beams at a 45° angle, each measuring 5.657 m in length. There are six sets of struts, spaced 2 m apart.

In accordance with the "Steel Strand for Prestressed Concrete" (GB/T 5224-2014) [34], we selected 1 × 7 unbonded prestressed hot-dip galvanized steel strands as the load-bearing cables, which have the following properties: tensile strength R_m = 1860 MPa, elastic modulus $E_0 = 1.95 \times 10^5$ MPa, linear expansion coefficient $\alpha_T = 1.17 \times 10^{-5}$/°C, and Poisson's ratio $\nu = 0.3$. The diameter of the support cables is 0.0127 m, while the wind-resistant cables have a diameter of 0.0152 m. The end support beams are made of HPB300 steel, with cross-sectional dimensions of 0.2 m in length and width, and a wall thickness of 0.01 m. The columns are constructed from Q355 seamless steel pipes, having an outer diameter of 0.2 m and an inner diameter of 0.05 m, with an elastic modulus of 2.06×10^5 N/mm^2. The struts are solid HPB300 steel rods with a diameter of 0.05 m. To simulate the PV panels, a virtual surface was employed, applying a uniform distributed load of 0.15 kN/m^2 to represent the self-weight of the PV modules. The geometric model of the flexible PV support system and the nomenclature of its components are illustrated in Figure 1.

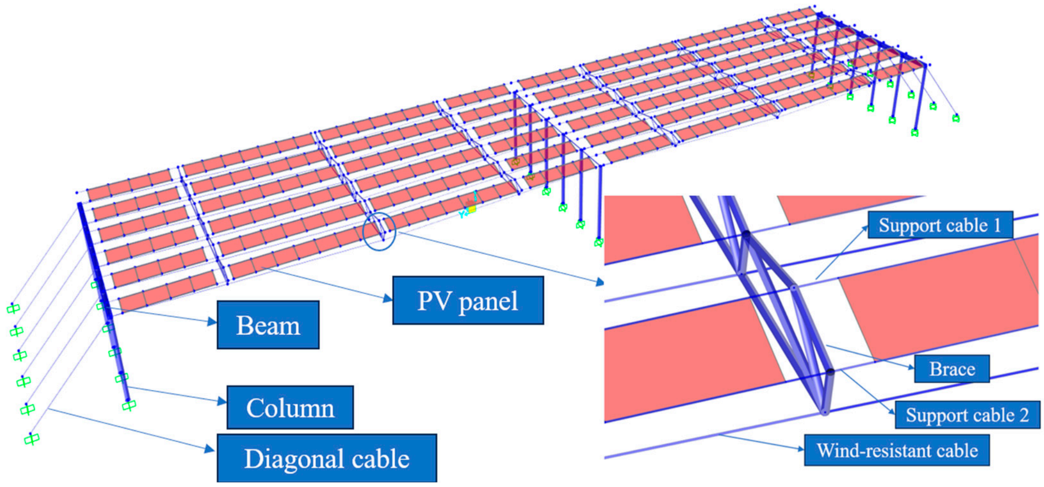

Figure 1. Geometric modeling and naming of flexible PV mounts.

2.2. Boundary Condition Configuration

For all components connected to the ground, the nodes are constrained in all six degrees of freedom (DOFs): translational in the x, y, and z directions, and rotational about the x, y, and z axes. The nodes along the upper edges on both sides of the flexible PV support structure are also fixed in all six DOFs. For the nodes on the middle support beams of the flexible PV structure, constraints are applied in the x and z directions. The sections of the columns interfacing with the ground are modeled using fixed supports to simulate full constraint conditions. Given the significant geometric nonlinearity inherent in the flexible PV support system, the analysis incorporates nonlinear approaches, specifically selecting the P-Δ effect and large displacement effects. The time step is set to 1000, with a time interval of 0.1 s. Given that the direct integration method is used for time–history analysis, Rayleigh damping is applied. Calculations yield a modal damping ratio of 0.02 for the first two modes, with the proportional damping coefficients $\alpha = 0.304$ and $\beta = 0.00132$.

2.3. Simulation of Fluctuating Wind Load Time History

The fluctuating wind speed time series $v(t)$ at time t is represented as a linear combination of the time series from several previous moments, plus an independent stochastic process at time t. The expression is as follows:

$$\nu(t) = \sum\nolimits_{k=1}^{p} \varphi \cdot \nu(t - k\Delta t) + N(t) \tag{1}$$

where $v(t)$ is the fluctuating wind speed at time t; φ_k is the autoregressive coefficient; p is the order of the AR model; $v(t - k\Delta t)$ is the fluctuating wind speed at k previous time steps; Δt is the time step of the fluctuating wind speed; and $N(t)$ is an independent stochastic process with a mean of 0 and variance σ_N^2. Multiplying both sides of Equation (2) by $v(t - k\Delta t)$ gives:

$$\nu(t)\nu(t - j\Delta t) = \sum\nolimits_{k=1}^{p} \varphi \cdot \nu(t - j\Delta t)(t - k\Delta t) + N(t) \cdot \nu(t - j\Delta t) \tag{2}$$

In Equation (3), $j = 1, 2, \ldots, p$. Taking the mathematical expectation on both sides of Equation (2)

$$E(v(t)v(t)) = \sum_{k=1}^{p} \varphi_k \cdot E(v(t - k\Delta t) \cdot v(t)) + \sigma_N^2 \tag{3}$$

Considering the properties of the autocorrelation function: the autocorrelation function of a stochastic process $X(t)$ is defined as the mean of $x(t)x(t+\tau)$. If the process is a stationary stochastic process, its mean $E[x(t)x(t+\tau)]$ is independent of the absolute value of time, and only depends on the time difference, that is:

$$R(j \cdot \Delta t) = E[v(t) \cdot v(t - j\Delta t)] \tag{4}$$

Since the mean of $N(t)$ is 0 and is independent of $v(t)$, the relationship between the correlation function $R(j \cdot \Delta t)$ and the autoregressive coefficient φ_k is:

$$R(j \cdot \Delta t) = \sum_{k=1}^{p} \varphi_k \cdot R[(t - k) \cdot \Delta t] \tag{5}$$

The autoregressive coefficients φ_k in the equation can be determined by the following system of equations:

$$\begin{cases} R(\Delta t) = \sum_{k=1}^{p} \varphi_k \cdot R[(1 - k) \cdot \Delta t] \\ R(2\Delta t) = \sum_{k=1}^{p} \varphi_k \cdot R[(2 - k) \cdot \Delta t] \\ \vdots \\ R(j\Delta t) = \sum_{k=1}^{p} \varphi_k \cdot R[(j - k) \cdot \Delta t] \end{cases} \tag{6}$$

where $R(j \cdot \Delta t)$ is the correlation function of the fluctuating wind speed at $t = j\Delta t$, which can be obtained by Fourier transform from the target power spectral density function, and can be calculated as follows:

$$R(\tau) = \int_0^{\infty} S(f) \cos(2\pi f \cdot t) dn \tag{7}$$

In Equation (6), f is the frequency of the fluctuating wind speed. Substituting the obtained autoregressive coefficients φ_k and the independent stochastic process $N(t)$ at time t into Equation (1), the single-point fluctuating wind speed time series can be obtained.

In MATLAB (2021b), programming was conducted to simulate the fluctuating wind speed time series for a single node based on the Davenport wind spectrum, utilizing the auto-regressive (AR) technique. The simulation does not account for the correlation of fluctuating wind speeds between different nodes. The duration of the fluctuating wind speed time series was set to 100 s with a time step of 0.1 s, and the AR model was configured with a fourth-order process. The standard wind speed was set to 30 m/s, and the frequency integration range was chosen from 0.001 Hz to 10 Hz [35]; the simulation results of the fluctuating wind flow are shown in Figure 2. As depicted in Figure 3, the simulated fluctuating wind speeds predominantly vary within the range of −10 m/s to 10 m/s, with a mean value oscillating around zero, indicating that the simulation results for the fluctuating wind are realistic and satisfactory. Furthermore, as shown in Figure 4, the simulated spectrum closely aligns with the target spectrum, demonstrating the efficacy of the AR method in replicating the desired wind speed characteristics.

The fluctuating wind speed time series for the flexible PV support structure was simulated using the linear filtering method. This time series was then converted into a fluctuating wind load time series. The relationship between wind speed and wind pressure is given by the following equation:

$$\omega = \frac{1}{2}\rho v^2 \tag{8}$$

In Equation (8), ω denotes the wind pressure corresponding to the wind speed; ρ represents the air density, assumed to be 1.225 kg/m^3 in this context; and v stands for the instantaneous wind speed. Utilizing the given equation and the relationship between the mean wind speed $\overline{v}$ and the fluctuating wind speed v_t, the time history of the fluctuating wind load can be derived.

$$F_t = \frac{1}{2}\rho\mu_s A\overline{v}^2 + \frac{1}{2}\rho\mu_s A\left(v_t^2 + 2\overline{v}v_t\right) \quad (9)$$

In Equation (9), μ_s is the shape coefficient, taken as 1.4 [36], and A represents the area of the PV panel. Figure 5 illustrates the time history of the fluctuating wind load. After this conversion, fluctuating wind can be added to SAP2000. The obtained data can be directly utilized for structural dynamic analysis in SAP2000.

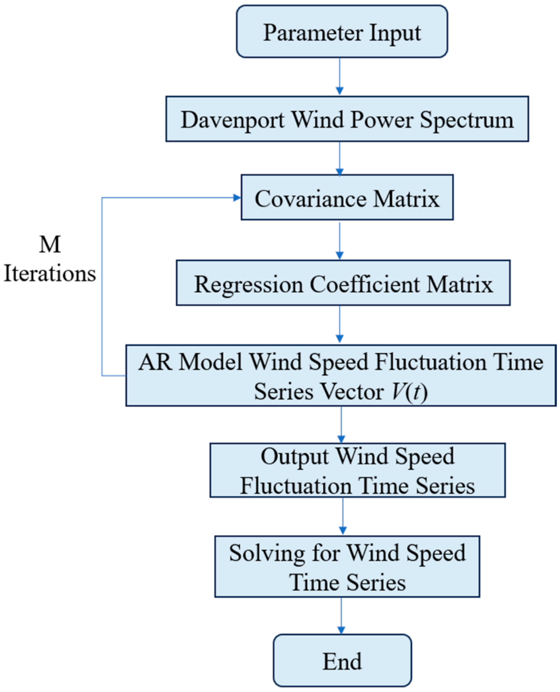

Figure 2. Fluctuating wind simulation process.

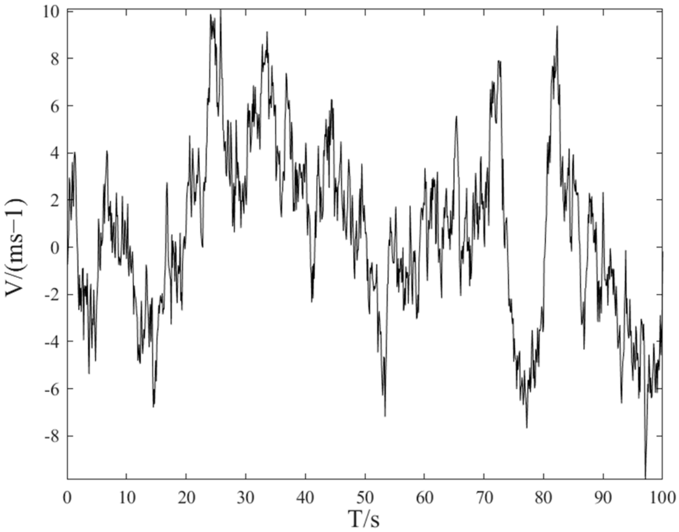

Figure 3. Fluctuating wind speed simulation spectrum.

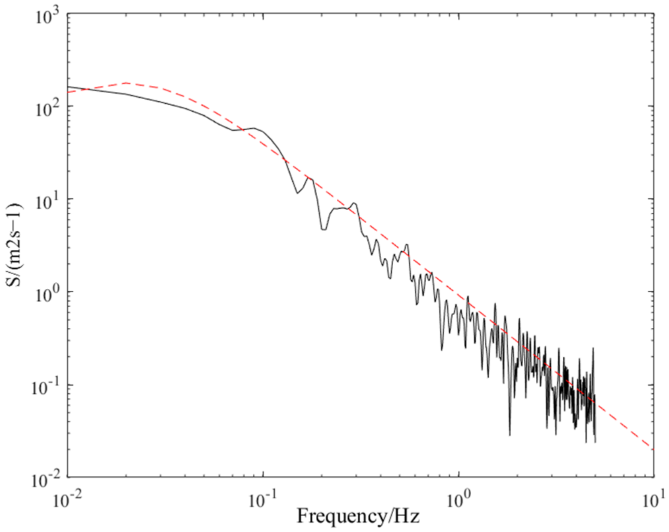

Figure 4. Fluctuating wind power spectrum vs. target spectrum.

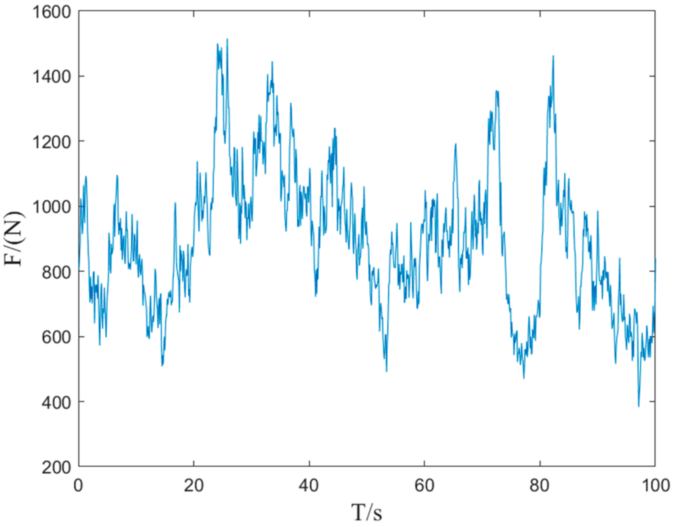

Figure 5. Fluctuating wind load time course.

3. Static Analysis of Flexible PV Racks for Extreme Working Conditions

To validate the accuracy of the numerical simulation, a comparative analysis with Li's [33] wind tunnel experiments was conducted. Wind speeds of 24 m/s, 28 m/s, 32 m/s, 36 m/s, 40 m/s, 44 m/s, 48 m/s, 49 m/s, and 50 m/s were selected for validation, and the results are depicted in the accompanying Figure 6. The maximum deviation occurs at 50 m/s, with an error of 16.8%. The mean error is calculated to be 9.1%, thereby demonstrating that the employed methodology can simulate the conditions with a high degree of accuracy.

3.1. Safety Analysis under Extreme Operating Conditions

For flexible PV brackets, the allowable deflection value adopted in current engineering practice is 1/100 of the span length [32]. To ensure the safety of PV modules under extreme static conditions, a detailed analysis of a series of extreme scenarios will be conducted. Given that the self-weight of the PV panels and flexible cables has a minimal impact on the flexible PV brackets, seismic loads are not considered. According to GB 50797-2012 "Code for Design of PV Power Stations" [37], the design value of the load effect combination should be calculated as follows:

$$S = \gamma_G S_{GK} + \gamma_w \psi_w S_{wk} + \gamma_S \psi_S S_{sk} + \gamma_t \psi_t S_{tk} \tag{10}$$

In Equation (10), S is the design value of the load effect combination; γ_G, γ_W, γ_S, γ_T are permanent load sub-factors, wind load sub-factors, snow load sub-factors and temperature load sub-factors, respectively; Ψ_W, Ψ_S, Ψ_T are the coefficients of the combined values of wind load, snow load, and temperature load, respectively; S_{GK}, S_w, S_{sk}, S_{tk} are the standard values of permanent load, wind load, snow load, and temperature load, respectively.

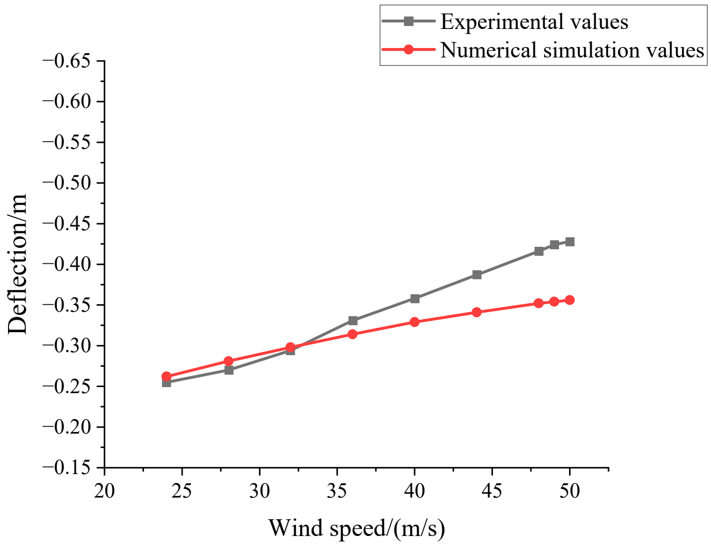

Figure 6. Comparison of maximum deflection values at different wind speeds.

According to the requirements of the aforementioned code, four types of ultimate limit state load combinations are presented in Table 1. Due to the unfavorable effects of permanent loads on the structure, γ_G is 1.2 for all four conditions.

Table 1. Extreme operating condition combinations.

Combination of Operating Conditions	$\gamma_W \boldsymbol{\Psi}_W$	$\gamma_S \boldsymbol{\Psi}_S$	$\gamma_T \boldsymbol{\Psi}_T$
1	1.4 × 1	0	1.4 × 0.6
2	0	1.4 × 1	1.4 × 0.6
3	1.4 × 0.6	0	1.4 × 1
4	0	1.4 × 0.6	1.4 × 1

Taking a flexible PV bracket with a span of 30 m and a cable axial force of 75 kN as the research object, we investigate the variation patterns of the support cables and wind-resistant cables under temperature decrease and increase scenarios. The calculation results shown in Figure 7 indicate that, regardless of a temperature decrease or increase, the axial force of the wind-resistant cables is greater than that of the support cables. Additionally, the axial force of the flexible cables during a temperature increase is less than that during a temperature decrease.

Selecting Case 1, with the deflection limit at the mid-span of the wind-resistant cable under temperature decrease conditions set to 1/100 of the span length as the standard, we investigate the prestress and span limits under extreme conditions. Spans of 15 m, 25 m, 30 m, 35 m, and 45 m were selected, along with various levels of prestress for plotting. As shown in Figure 8, when the span exceeds 30 m, the rate of deflection increase accelerates with the increase in the span length.

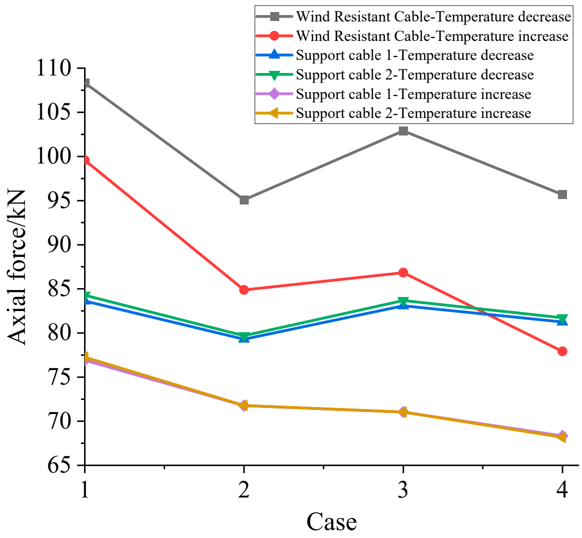

Figure 7. Comparison of axial forces in wind-resistant cables and support cables under different conditions of temperature increase and decrease.

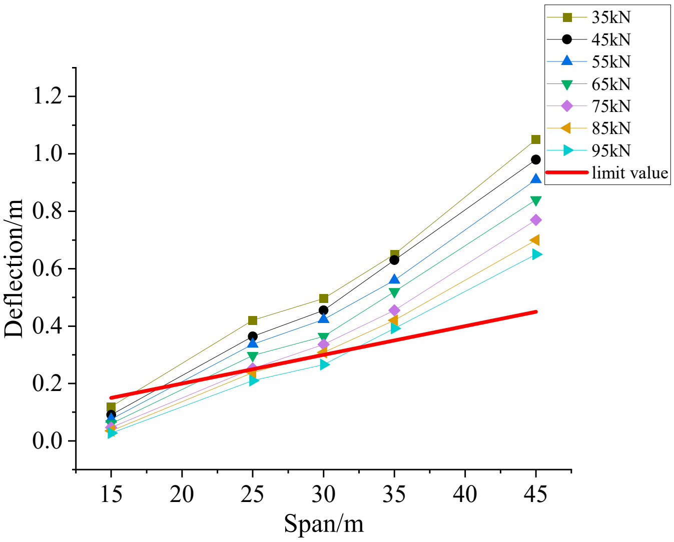

Figure 8. Comparison of mid-span deflections with different spans and prestresses.

Table 2 presents the prestress limits for different spans under extreme conditions. It is essential to consider the minimum prestress value corresponding to each span length when designing flexible PV brackets.

Table 2. The prestress limits under different span lengths.

Span/m	**15**	**25**	**30**	**35**	**45**
Limit value of prestress/kN	27	75	85	105	154

3.2. Critical Wind Speed Study

In summary, the study on the critical wind speed of flexible photovoltaic brackets uses the mid-span deflection limit at the wind-resistant cables under cooling conditions as the standard, set at 1/100 of the span length. Figure 9 illustrates the critical wind speed for distinct prestressing and span combinations. As illustrated in Figure 8, the critical wind speed exhibits a linear increase with increasing prestress, while the rate of increase diminishes with the increasing span. When the span of the flexible PV bracket is 45 m and the prestressing force is 35 kN, the critical wind speed decreases significantly due to the fact that the self-weight of the flexible PV bracket represents a considerable proportion of the pre-stressing cords, which are insufficient to cope with the wind load while counteracting the self-weight. Therefore, it is essential to ensure that the prestressing force of the flexible cords is greater than 45 kN in order to prevent failure.

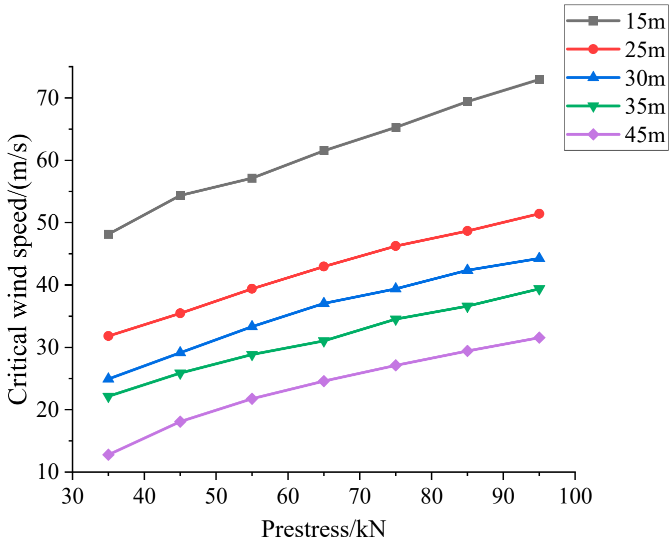

Figure 9. Critical wind speed for different spans and prestress combinations.

Table 3 presents the specific values of critical wind pressure for different spans and prestressing combinations. It is of paramount importance to exercise particular caution when designing flexible PV mounts in accordance with the specific characteristics of the local environment. This approach will ensure the safety of the mounting system while simultaneously reducing costs.

Table 3. The critical wind pressure values under different combinations of span lengths and prestress levels (kN/m^2).

Span/m		15	25	30	35	45
Prestress/kN	35	1.42	0.62	0.38	0.30	0.1
	45	1.81	0.77	0.52	0.41	0.2
	55	2.00	0.95	0.60	0.51	0.29
	65	2.32	1.13	0.64	0.59	0.37
	75	2.61	1.31	0.76	0.73	0.45
	85	2.95	1.45	1.1	0.82	0.53
	95	3.26	1.62	1.2	0.95	0.61

Based on the data in Figure 8, the critical wind speed equations are given for prestressing of 35 kN to 95 kN (not applicable when the span is 45 m and prestressing is 35 kN):

$$V_{\max} = A_1 x + B_1 \tag{11}$$

In Equation (11), $V_{\max}$ is the critical wind speed, x is the span, and the values of a and b are given in Table 4 below:

Table 4. Values of A and B in different spans.

Span/m	15	25	30	35	45
A_1	0.413	0.327	0.323	0.288	0.270
B_1	33.700	20.375	13.614	12.067	5.931

3.3. Modal Analysis of Flexible PV Mounts

The eigenvector method in SAP2000 was employed to analyze the natural vibration characteristics of a flexible PV support structure after the application of prestress. The frequencies of the first 12 modes are shown below. Given that fluctuating wind load is a type of random load that varies randomly over time, with a period of 1 to 2 s and a frequency of 0.5 Hz to 1 Hz, the minimal natural frequency, as indicated in Table 5, is 1.460 Hz. This frequency is higher than that of the fluctuating wind, and the structure's natural frequencies are 1.460 to 6.032 times greater than the fluctuating wind frequency. According to vibration theory, resonance does not occur when the frequency of external excitation differs by more than 25% from the natural frequency of the structure. Therefore, resonance will not occur in the flexible PV support structure.

Table 5. Frequency of the first 12 orders of vibration pattern of flexible PV mounts.

Modal Step	Natural Period/s	Natural Frequency/Hz
1	0.685	1.460
2	0.646	1.547
3	0.641	1.560
4	0.635	1.575
5	0.629	1.589
6	0.613	1.630
7	0.598	1.673
8	0.587	1.702
9	0.553	1.807
10	0.460	2.172
11	0.353	2.835
12	0.331	3.016

As shown in Table 6, the first mode primarily exhibits translational vibration in the x-direction, while the fourth and eighth modes primarily exhibit translational vibration in the z-direction. The second, third, fifth, sixth, seventh, ninth, tenth, eleventh, and twelfth modes primarily exhibit torsional vibration.

Table 6. Modal participation factors.

Modal Step	UX	UY	UZ	RZ
1	−2.413318	0.000583	0.095626	−1.116369
2	−0.079541	−0.010703	−0.250148	5.499972
3	0.258653	0.002853	0.424804	−27.059293
4	−0.023301	0.001903	−1.546522	−1.364577
5	0.118711	0.004366	0.383939	30.625138
6	−0.086721	0.004188	−1.00108	−1.768091
7	−0.00158	−0.006285	−0.237825	−2.309102
8	0.046369	−0.000467	1.035485	−0.556642
9	−0.196866	0.000431	0.502407	−5.998283
10	0.104026	−0.001627	−0.165358	−2.266144
11	0.004583	0.000024	0.000638	−0.086253
12	−0.000871	0.003654	0.000046	−2.483576

3.4. Wind Vibration Response of Flexible PV Mounting Structures

To investigate the impact of fluctuating wind loads on the flexible PV support structure, the previously obtained wind load time histories were applied to a flexible PV support structure with a span of 30 m and a prestress of 50 kN. Analysis of the calculation results shows that the maximum deflection and acceleration occur at the mid-span, and the axial force in the wind-resistant cables is greater than that in the supporting cables. Figure 10 presents the time histories of mid-span deflection, acceleration, and wind-resistant cable axial force under wind-suction and wind-pressure conditions. The axial force in the wind-resistant cables is greater under wind-pressure conditions than under wind-suction conditions. The displacement time history at the mid-span is greater under wind-pressure conditions than under wind-suction conditions. However, for mid-span acceleration, the wind suction condition results in greater values than the wind-pressure condition. Overall, it can be concluded that the flexible PV support structure exhibits a consistent response trend under both wind-suction and wind-pressure conditions.

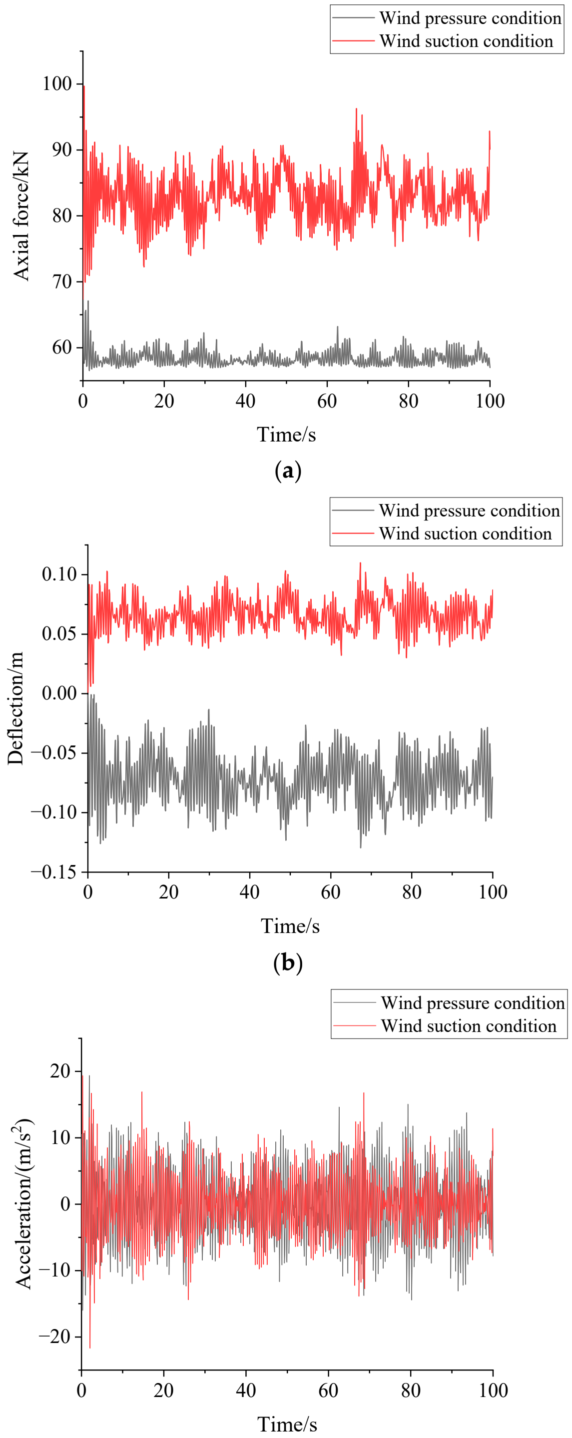

(**a**)

(**b**)

(**c**)

Figure 10. Wind-induced vibration response of the flexible PV mounting structure under wind-suction and wind-pressure conditions. (**a**) Time history of axial force of wind-resistant cables. (**b**) The mid-span deflection time history. (**c**) The mid-span acceleration time history.

To investigate the distribution patterns of maximum deflection, axial force, and acceleration in a flexible PV array group, Tables 7 and 8, respectively, present the comparisons of average deflection, average axial force, and absolute average acceleration at the mid-span under wind-suction and wind-pressure conditions. The tables indicate that the maximum wind-induced vibration responses in the flexible PV array group occur at the mid-span under both wind suction and wind-pressure conditions, with the responses gradually decreasing towards the edges under wind-pressure conditions.

Table 7. Comparison of deflection, axial force, and acceleration at mid-span of different rows for wind-pressure conditions.

	First Row	Second Row	Third Row	Fourth Row	Fifth Row	Sixth Row
Axial force/kN	76.99	78.75	79.04	77.15	78.97	77.6
Deflection/m	−0.287	−0.295	−0.303	−0.310	−0.288	0.07
Acceleration/(m/s^2)	3.97	3.54	4.86	3.67	3.49	4.93

Table 8. Comparison of deflection, axial force, and acceleration at mid-span of different rows under wind-suction conditions.

	First Row	Second Row	Third Row	Fourth Row	Fifth Row	Sixth Row
Axial force/kN	48.55	48.26	49.28	48.41	49.01	47.88
Deflection/m	0.213	0.212	0.184	0.205	0.186	−0.08
Acceleration/(m/s^2)	4.93	3.96	5.24	3.96	4.55	4.90

Based on the summarized results, in subsequent reinforcement of the flexible PV mounting structure, it is recommended to focus on the mid-span of the central rows for the analysis of deflection, axial force, and acceleration. For axial force analysis, focus on the axial force in the wind-resistant cables.

4. Wind-Induced Vibration Coefficient for Flexible PV Mounting Structure

Although the finite element method can quantitatively analyze the dynamic response of flexible PV support structures under fluctuating wind loads, this method's time consumption is highly dependent on computer performance and is often impractical for actual engineering design. To better meet practical application needs, it is necessary to consider using static calculation methods to determine the dynamic response of structures.

In practical engineering design, equivalent static wind loads are commonly used to account for the dynamic effects of wind. The equivalent static wind load is represented by the product of the static wind load P_s and the wind vibration coefficient β. According to the Chinese "Building Structural Load Specification" [38], the wind vibration coefficient β can be taken as the load wind-vibration coefficient β_{Li}, which is expressed as follows:

$$\beta_L = 1 + \frac{P_d}{P_s} = 1 + \frac{\mu \sigma_F}{P_s} \tag{12}$$

$$\sigma_F = \sqrt{\frac{\sum_{n=1}^{N} (P_d - P_s)^2}{n}} \tag{13}$$

In Equation (12), P_d represents the nodal dynamic wind load. P_s is the nodal static wind load. μ is the peaking factor, which takes the value of 3.5, according to the wind-resistant design calculation manual [39]. σ_F is the mean square deviation of the fluctuating wind response.

In addition to the load wind-vibration coefficient, which is a commonly used wind-vibration coefficient, there is also a displacement wind-vibration coefficient and a displacement of the structure in the time domain. The displacement of the structure in the time domain is made up of static displacement caused by the average wind and dynamic displacement caused by fluctuating wind. The displacement wind-vibration coefficient is calculated using the following formula:

$$\beta_u = \frac{\overline{u} + \hat{u}}{\overline{u}} = 1 + \frac{\hat{u}}{\overline{u}} = 1 + \frac{\mu\sigma_w}{\overline{u}} \tag{14}$$

In Equation (14), β_{ui} is the displacement wind-vibration coefficient, $\hat{u}$ is the peak displacement due to the fluctuating wind, $\overline{u}$ is the static displacement due to the mean wind, and σ_{w} is the mean square deviation of the displacement response to the fluctuating wind.

$$\sigma_w = \sqrt{\frac{\sum_{n=1}^{N}(\hat{u} - \overline{u})^2}{n}} \tag{15}$$

Given that the fluctuating wind load time duration is in the hundreds of seconds, with a time step of 0.1 s, the value of N is taken to be 1000.

To minimize the error between the load wind-vibration coefficient and the displacement wind-vibration coefficient, 10 different sets of fluctuating wind speed time histories were used to calculate the load wind-vibration coefficient and the displacement wind-vibration coefficient under wind-suction and wind-pressure conditions. The simulation was conducted with a span of 30 m, and axial forces of 50 kN in both the supporting cables and the wind-resistant cables. Refer to previous for other material properties and settings.

Table 9 indicates that the displacement wind-vibration coefficients under both wind-suction and wind-pressure conditions are generally higher than the load wind-vibration coefficients. This suggests that the deflection of the flexible PV support structure is more sensitive to fluctuating wind loads compared to the axial force. Considering the safety of flexible PV support structures, it is reasonable to use the displacement wind-vibration coefficient rather than the load wind-vibration coefficient. For the flexible PV arrays with wind-resistant cables discussed in this study, a recommended range for the wind-vibration coefficient is 1.5 to 2.52. This range aligns well with the suggested wind-vibration coefficient values of 1.2 to 2.5 obtained from wind tunnel tests [31], thereby further validating the accuracy of the numerical simulations presented in this paper.

Table 9. Comparison of load wind-vibration coefficients and displacement wind-vibration coefficients for different fluctuating wind speeds with range wind pressure and wind suction conditions.

Group Number	Wind Pressure Condition		Wind Suction Condition	
	β_L	β_u	β_L	β_u
1	1.256	1.564	1.159	2.173
2	1.218	1.556	1.112	2.110
3	1.243	1.604	1.118	2.230
4	1.248	1.626	1.123	2.294
5	1.225	1.571	1.114	2.133
6	1.224	1.611	1.114	2.132
7	1.235	1.586	1.110	2.149
8	1.217	1.540	1.125	2.179
9	1.228	1.561	1.114	2.148
10	1.193	1.490	1.103	2.046

5. Reinforcement Scheme for Wind-Induced Vibration Resistance in Flexible PV Mounting Structures

Given the sensitivity of flexible PV support structures to wind loads and their pronounced wind-induced vibration responses in large-span settings, the development of effective vibration control measures is of paramount importance. This study proposes and evaluates several reinforcement strategies for flexible PV support structures.

The baseline, unreinforced flexible PV support structure is designated as F. The first reinforcement strategy involves increasing the diameter of the prestressed cables to 17.8 mm and 21.6 mm, respectively. These configurations are named F1-1 and F1-2 for ease of comparison. The second strategy (F2) introduces a support beam at mid-span, constructed from Q355 seamless steel pipes with an outer diameter of 0.2 m and an inner diameter of 0.05 m. The third strategy (F3) involves adding a stabilizing cable at mid-span, with a diameter of 0.0287 m and a horizontal tension of 15.9 kN. The structural response varies depending on the reinforcement strategy and loading conditions. For strategy F2, the support beam directly impacts the mid-span, causing the maximum deflection and acceleration to occur at the 3/4L or 1/4L positions of the middle row. Conversely, in strategy F3, the stabilizing cable causes the maximum deflection and acceleration to appear at the L/4 or 3L/4 positions of the middle row under wind-suction conditions. However, under wind-pressure conditions, the maximum deflection and acceleration remain at mid-span. The remaining material properties and setup are simulated according to the parameters detailed in Section 2. Geometric schematics of the wind-induced vibration control strategies F2 and F3 are shown in Figures 11 and 12.

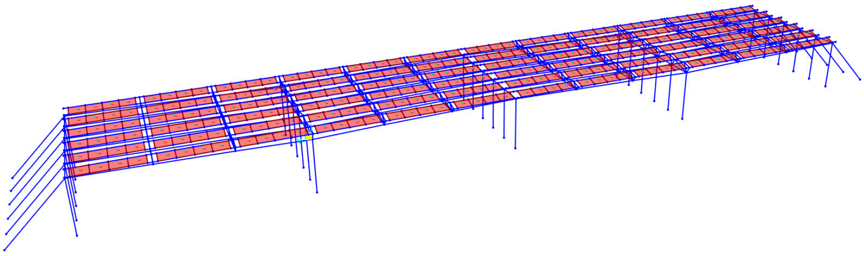

Figure 11. F2 Geometric model of wind-vibration resistance scheme.

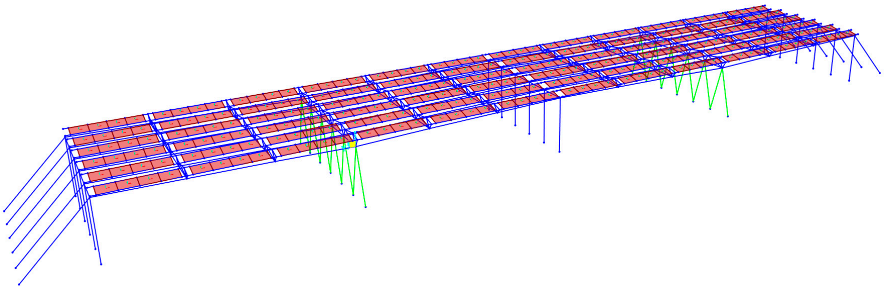

Figure 12. F3 Geometric model of wind-vibration resistance scheme.

Figures 13 and 14 illustrate the dynamic responses of a flexible PV support structure under wind-pressure and wind-suction conditions, respectively. Under wind-pressure conditions: For the axial force in the flexible cables of the structure, the hierarchy is as follows: F1-2 > F1-1 > F > F3 > F2. Increasing the diameter of the prestressed cables significantly enhances the axial force in the flexible cables. Regarding the maximum deflection of the structure, the order is: F3 > F > F1-1 > F1-2 > F2. The deflection in F3 is greater than in the unstiffened flexible PV support structure because the stabilizing cables in F3 are tensioned but not compressed. For structural acceleration, the ranking is: F3 > F > F1-1 > F1-2 > F2.

Under wind-suction conditions: For the axial force in the flexible cables, the sequence is: F3 > F2 > F > F1-1 > F1-2. The presence of stabilizing cables increases the axial force. Regarding the maximum deflection of the structure, the order is: F > F1-1 > F1-2 > F3 > F2. For structural acceleration, the ranking is: F3 > F > F1-1 > F1-2.

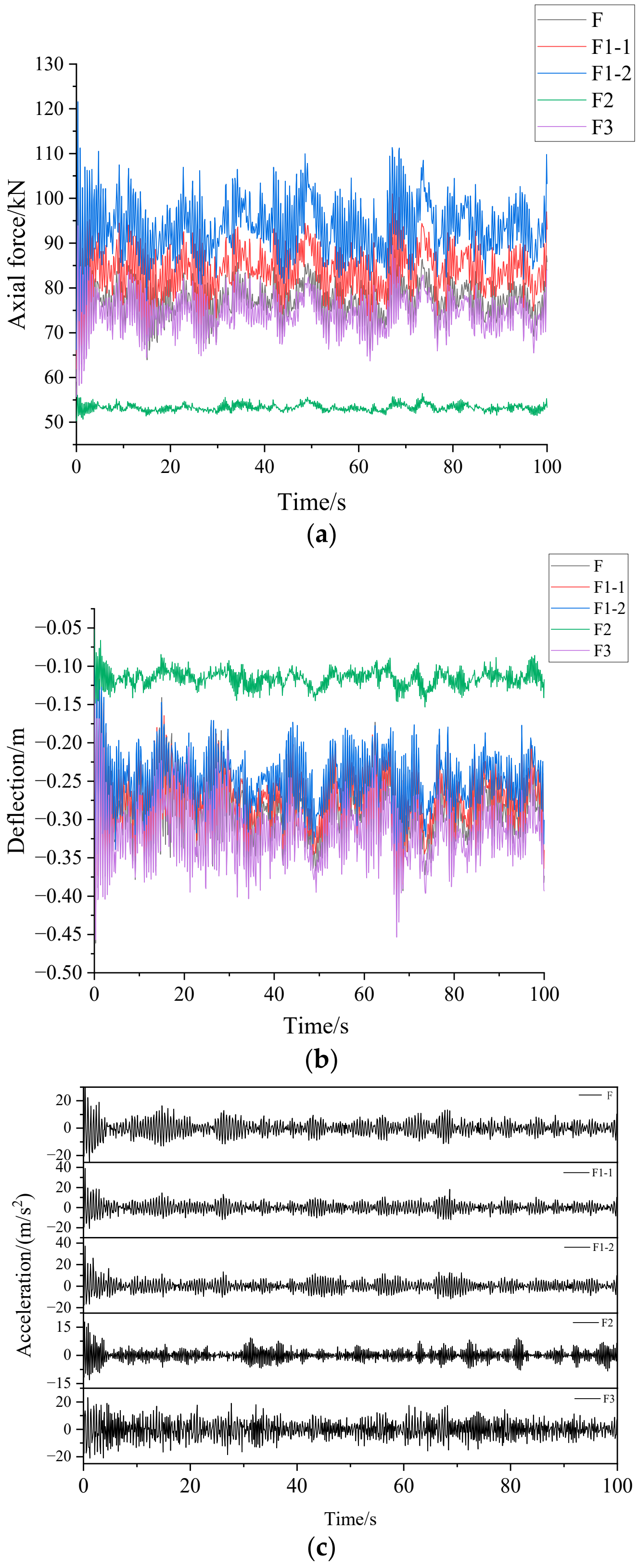

Figure 13. A comparative analysis of the wind-pressure response time history of various structural strengthening schemes. (**a**) Comparison of axial force. (**b**) Deflection comparison. (**c**) Acceleration comparison.

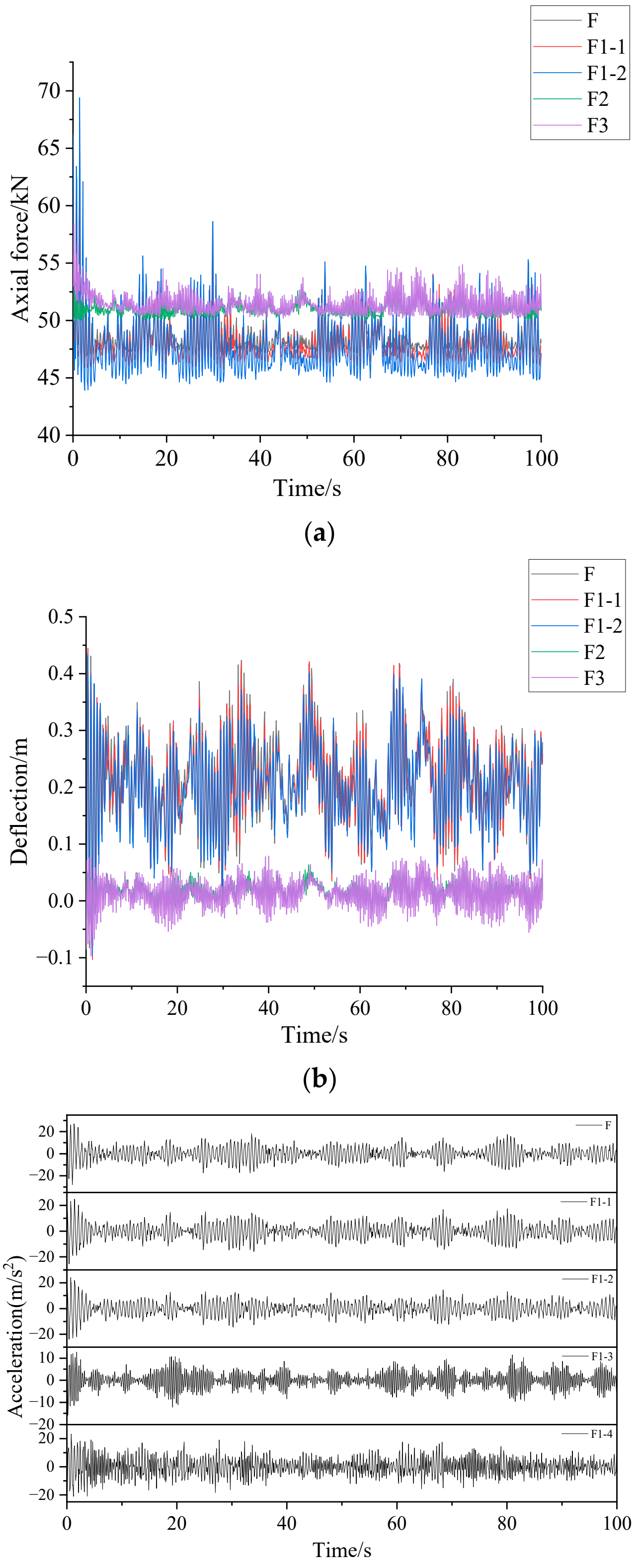

(**a**)

(**b**)

(**c**)

Figure 14. A comparative analysis of the wind-absorption response time histories of different structural reinforcement schemes. (**a**) Comparison of axial force. (**b**) Deflection comparison. (**c**) Acceleration comparison.

Figures 15 and 16 illustrate the ratios of wind-induced vibration responses—namely, axial force, deflection, and acceleration—under wind-pressure and wind-suction conditions, compared to the unreinforced flexible PV mounting structure. To better demonstrate the effectiveness of each reinforcement scheme, Tables 10 and 11 provide the specific ratios of each scheme relative to the unreinforced case. The F2 scheme is the most effective in reducing the wind-induced vibration response of the structure. In contrast, the F3 scheme is less beneficial, as it may even be detrimental in reducing the structural wind-induced vibration response. Although the F1-1 and F1-2 schemes do contribute to reducing the response, their impact is not significant. Similarly, under wind-suction conditions, the F2 scheme remains the most effective in mitigating the structural wind-induced vibration response, followed by the F3 scheme. The F1-1 and F1-2 schemes also help to reduce the wind-induced vibration response, but their effectiveness is even less pronounced under wind-suction conditions. These findings highlight that while F2 provides the most substantial reduction in wind-induced vibration for both conditions, the F3 scheme, though less effective for wind pressure, offers a cost-efficient and space-saving alternative with better performance under wind-suction conditions. Conversely, the F1-1 and F1-2 schemes, although slightly effective, do not provide significant benefits in either condition.

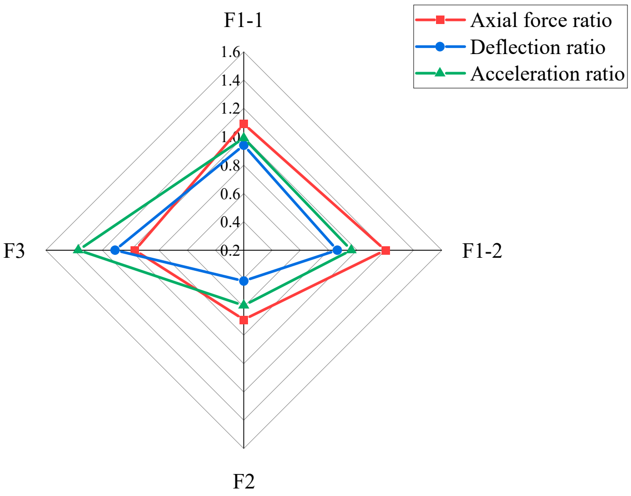

Figure 15. Comparison of wind vibration response of optimization schemes for wind-pressure conditions.

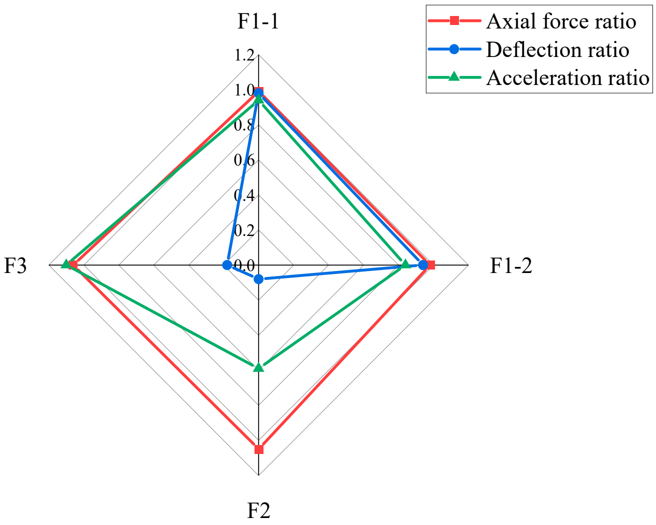

Figure 16. Comparison of wind vibration response of optimization schemes for wind suction condition.

Table 10. Comparison of wind-pressure conditions by scenario.

	F1-1	**F1-2**	**F2**	**F3**
Axial force ratio	1.09	1.20	0.69	0.97
Deflection ratio	0.94	0.861	0.418	1.11
Acceleration ratio	0.99	0.96	0.59	1.37

Table 11. Comparison of wind suction scenarios.

	F1-1	**F1-2**	**F2**	**F3**
Axial force ratio	0.99	0.98	1.05	1.06
Deflection ratio	0.98	0.94	0.08	0.18
Acceleration ratio	0.94	0.84	0.59	1.1

In summary, although the F2 scheme is the most effective in reducing the wind-induced vibration response of the structure, it requires more land area and typically incurs higher costs. The F1-1 and F1-2 schemes, while capable of mitigating the wind-induced vibration response, do not significantly reduce the response under both wind-pressure and wind-suction conditions. The F3 scheme effectively reduces the structural wind-induced vibration response under wind-suction conditions, but it is less effective for wind-pressure conditions. Compared to F2, F3 has a lower cost and is more land-efficient.

6. Conclusions

Using MATLAB, we developed a program to generate the fluctuating wind-speed time series, and then created a model in SAP2000 to conduct both static analysis under extreme conditions and wind-induced vibration response analysis. This research focused on the safety and critical wind speed of flexible PV mounting structures, as well as the calculation of wind-vibration coefficients, and proposed reinforcement strategies for wind-induced vibration resistance. The results indicate the following:

(1) Under the combined effect of extreme conditions, the axial force of the wind-resistant cable during a temperature rise is lower than that of the flexible cable during a temperature drop. Extreme conditions dominated by wind have a greater impact on the flexible PV mounting structures compared to those dominated by snow. For structures with spans of 15 m, 25 m, 30 m, 35 m, and 45 m, the prestress limits under extreme conditions are 27 kN, 75 kN, 85 kN, 105 kN, and 154 kN, respectively.

(2) Modal analysis reveals that the structure does not resonate under fluctuating wind loads, with the dominant vibration mode being torsional. The mid-span displacement and axial force in the wind-resistant cables are greater under wind-pressure conditions than under wind-suction conditions. In contrast, the mid-span acceleration is higher under wind-suction conditions compared to wind-pressure conditions.

(3) The calculation of displacement and load wind-vibration coefficients indicates that using the displacement wind-vibration coefficient is more appropriate than using the load wind-vibration coefficient. It is recommended that the wind-vibration coefficient be in the range of 1.5 to 2.52.

(4) Four structural reinforcement schemes were proposed for enhancing the wind-induced vibration resistance of flexible PV mounting structures. The analysis suggests that adding a support beam at the mid-span is the most effective measure to reduce the structural wind-vibration response. However, this approach requires more land and usually entails higher costs. Increasing the cable diameter can reduce the structural wind-vibration response, but the reduction is not significant when considering both the wind-pressure and wind-suction conditions. Adding a stabilizing cable at the mid-span effectively reduces the wind-vibration response under wind-suction conditions but is less effective for wind-pressure conditions. Compared to adding support beams, this method can be more cost-effective and requires less land area.

Author Contributions: Conceptualization, Y.L.; methodology, Y.L.; software, Y.L.; validation, Y.L. and J.Z.; formal analysis, J.Z.; investigation, Y.L. and Y.P.; resources, J.Z.; data curation, Y.L. and Y.P.; writing—original draft preparation, Y.L.; writing—review and editing, J.Z. and Y.P.; visualization, Y.L.; supervision, J.Z.; project administration, J.Z.; funding acquisition, J.Z. All authors have read and agreed to the published version of the manuscript.

Funding: This research was funded by the National Natural Science Foundation of China (Grant No. 52201323).

Data Availability Statement: The data presented in this study are available on request from the corresponding author.

Acknowledgments: This work is supported by the National Natural Science Foundation of China. This support is gratefully appreciated.

Conflicts of Interest: The authors declare no conflicts of interest.

References

1. Liu, H.J.; Shi, J.; Guo, L.X.; Qiao, L.C. China's Energy Reform in the New Era: Process, Achievements and Prospects. *J. Manag. World* **2022**, *38*, 6–24. [CrossRef]
2. Wang, C.; Shuai, J.; Ding, L.; Lu, Y.; Chen, J. Comprehensive benefit evaluation of solar PV projects based on multi-criteria decision grey relation projection method: Evidence from 5 counties in China. *Energy* **2022**, *238*, 121654. [CrossRef]
3. Wang, L. Photovoltaic industry is expected to usher in a new round of outbreak. *China Bus. News*, 10 November 2020; p. 005. [CrossRef]
4. Ren, G.; Wan, J.; Liu, J.; Yu, D. Spatial and temporal assessments of complementarity for renewable energy resources in China. *Energy* **2019**, *177*, 262–275. [CrossRef]
5. Wang, Y. PV module flexible bracket technical solution. *Sol. Energy* **2018**, 37–40.
6. Liu, X.J.; Cui, G.Q.; Yu, K. Research on Solar Photovoltaic Flexible Racking System. *New Technol. New Prod. China* **2020**, 79–81. [CrossRef]
7. Aly, A.; Bitsuamlak, G. Aerodynamics of ground-mounted solar panels: Test model scale effects. *J. Wind Eng. Ind. Aerodyn.* **2013**, *123*, 250–260. [CrossRef]
8. Aly, A.; Bitsuamlak, G. Wind induced pressures on solar panels mounted on residential homes. *J. Archit. Eng.* **2014**, *20*, 04013003. [CrossRef]
9. Kopp, G.A.; Banks, D. Use of wind tunnel test method for obtaining design wind loads on roof-mounted solar arrays. *J. Struct. Eng.* **2013**, *139*, 284–287. [CrossRef]
10. Pratt, R.N.; Kopp, G.A. Velocity measurements around low-profile, tilted, solar arrays mounted on large flat-roofs, for wall normal wind directions. *J. Wind Eng. Ind. Aerodyn.* **2013**, *123*, 226–238. [CrossRef]
11. Stathopoulos, T.; Zisis, I.; Xypnitou, E. Local and overall wind pressure and force coefficients for solar panels. *J. Wind Eng. Ind. Aerodyn.* **2014**, *125*, 195–206. [CrossRef]
12. Warsido, W.P.; Bitsuamlak, G.T.; Barata, J. Influence of spacing parameters on the wind loading of solar array. *J. Fluids Struct.* **2014**, *48*, 295–315. [CrossRef]
13. Shafique, M.; Luo, X.; Zuo, J. Photovoltaic-green roofs: A review of benefits, limitations, and trends. *Sol. Energy* **2020**, *202*, 485–497. [CrossRef]
14. Trindade, A.; Cordeiro, L. Automated formal verification of stand-alone solar photovoltaic systems. *Sol. Energy* **2019**, *193*, 684–691. [CrossRef]
15. Glick, A.; Smith, S.E.; Ali, N.; Bossuyt, J.; Recktenwald, G.; Calaf, M.; Cal, R.B. Influence of flow direction and turbulence intensity on heat transfer of utility-scale photovoltaic solar farms. *Sol. Energy* **2020**, *207*, 173–182. [CrossRef]
16. Naeiji, A.; Raji, F.; Zisis, I. Wind loads on residential scale rooftop photovoltaic panels. *J. Wind. Eng. Ind. Aerodyn.* **2017**, *168*, 228–246. [CrossRef]
17. Mignolet, M.P.; Spanos, P.D. Simulation of Homogeneous Two-Dimensional Random Fields: Part IAR and ARMA Models. *J. Appl. Mech.* **1992**, *59*, S260–S269. [CrossRef]
18. Owen, J.S.; Eccles, B.J.; Choo, B.S.; Woodings, M.A. The application of auto-regressive time series modelling for the: Time-frequency analysis of civil engineering structures. *Eng. Struct.* **2001**, *23*, 521–536. [CrossRef]
19. Borgman, L.E. *Ocean Wave Simulation for Engineering Design*; American Society of Civil Engineers: Reston, VA, USA, 1967; p. 95.
20. Shinozuka, M. Simulation of Multivariate and Multidimensional Random Processes. *J. Acoust. Soc. Am.* **1971**, *49*, 357–368. [CrossRef]
21. Shinozuka, M.; Jan, C.M. Digital simulation of random processes and its applications. *J. Sound Vib.* **1972**, *25*, 111–128. [CrossRef]
22. Yamada, M.; Ohkitani, K. Orthonormal wavelet analysis of turbulence. *Fluid Dyn. Res.* **1991**, *8*, 101–115. [CrossRef]
23. Kitagawa, T.; Nomura, T. A wavelet-based method to generate artificial wind fluctuation data. *J. Wind. Eng. Ind. Aerodyn.* **2003**, *91*, 943–964. [CrossRef]
24. Tang, S.L.; Luo, Y.F. Development and application of artificial neural network technology. *Comput. Dev. Appl.* **2009**, *2*, 10.

25. Mao, J.; Zhao, H.D.; Yao, J.J. Application and prospect of Artificial Neural Network. *Electron. Des. Eng.* **2011**, *19*, 6265.
26. Guo, T.; Yang, Y.; Huang, G.Q.; Zhang, J.M. Wind-induced vibration analysis of flexible photovoltaic support structure under mountain canyon terrain. *Acta Energiae Solaris Sin.* **2023**, *44*, 31–40. [CrossRef]
27. Cai, Y.; Deng, H.; Li, B.Y. Wind-resistant design method of cable-suspended photovoltaic module support structures. *J. Vib. Shock* **2022**, *41*, 69–77.
28. Xie, D.; Fan, J. Wind vibration analysis of prestressed flexible photovoltaic support systems. *Build. Struct.* **2021**, *51*, 15–18.
29. Wang, Z.G.; Zhao, F.F.; Ji, C.M.; Peng, X.F.; Lu, H.Q. Wind-induced vibration analysis of multi-row and multi-span flexible photovoltaic support. *Eng. J. Wuhan Univ.* **2021**, *54*, 75–79.
30. He, X.-H.; Ding, H.; Jing, H.-Q.; Zhang, F.; Wu, X.-P.; Weng, X.-J. Wind-induced vibration and its suppression of photovoltaic modules supported by suspension cables. *J. Wind. Eng. Ind. Aerodyn.* **2020**, *206*, 104275. [CrossRef]
31. Xu, H.; Ding, K.; Shen, G.; Du, H.; Chen, Y. Experimental investigation on wind-induced vibration of photovoltaic modules supported by suspension cables. *Eng. Struct.* **2024**, *299*, 117125. [CrossRef]
32. Liu, J.; Li, S.; Luo, J.; Chen, Z. Experimental study on critical wind velocity of a 33-meter-span flexible photovoltaic support structure and its mitigation. *J. Wind. Eng. Ind. Aerodyn.* **2023**, *236*, 105355. [CrossRef]
33. Li, W.; Ke, S.; Cai, Z.; Ji, C.; Wang, W.; Wang, L.; Ren, H. Instability mechanism and failure criteria of large-span flexible PV support arrays under severe wind. *Sol. Energy* **2023**, *264*, 112000. [CrossRef]
34. *GB/T 5224-2014*; Steel Strand for Prestressed Concrete. China Standard Publishing House: Beijing, China, 2015.
35. Zhang, Z.H. Simulation of wind loading. *J. Build. Struct.* **1994**, 44–52.
36. Zhang, J.; Lou, Y. Study of Wind Load Influencing Factors of Flexibly Supported Photovoltaic Panels. *Buildings* **2024**, *14*, 1677. [CrossRef]
37. *GB 50797-2012*; Code for Design of Photovoltaic Power Station. Standardization Administration of the People's Republic of China: Beijing, China, 2012.
38. *GB 50009-2012*; Building Structural Load Specification. Standardization Administration of the People's Republic of China: Beijing, China, 2012.
39. Zhang, X.T. *Engineering Wind Design Calculation Manual*; China Construction Industry Press: Beijing, China, 1998.